analytical chemistry

pubs.acs.org/ac
Article

Trifluoroacetic Acid as a Molecular Probe for the Dense Phase in Liquid−Liquid Phase-Separating Peptide Systems

Jessica Lim, SzeYuet Chin, Ali Miserez,* Kai Xue,* and Konstantin Pervushin*

Cite This: https://doi.org/10.1021/acs.analchem.4c03444
Read Online

ABSTRACT: Although trifluoroacetic acid (TFA) is not typically considered a Hofmeister reagent, it has been demonstrated to modulate biocoacervation. We show that TFA can be employed to probe specific interactions in coacervating bioinspired peptide phenylalanine (Phe) ^{19}F-labeled at a single site, altering its liquid−liquid phase separation (LLPS) behavior. Solid-state nuclear magnetic resonance (NMR) spectroscopy revealed two dynamically distinct binding modes of TFA with Phe, resulting in a structured, dipolar-ordered complex and a more dynamic complex, highlighting the proximity between TFA and Phe. Quantum chemistry modeling of ^{19}F chemical shift differences indicates that the structured complex is formed by the intercalation of one TFA molecule between two stacked Phe aromatic rings, possibly contributing to the stabilization of the condensed dense phase. Thus, we propose that TFA can be used as a convenient molecular probe in ^{19}F NMR-based studies of the structure and dynamics of the dense phase in LLPS peptide systems.

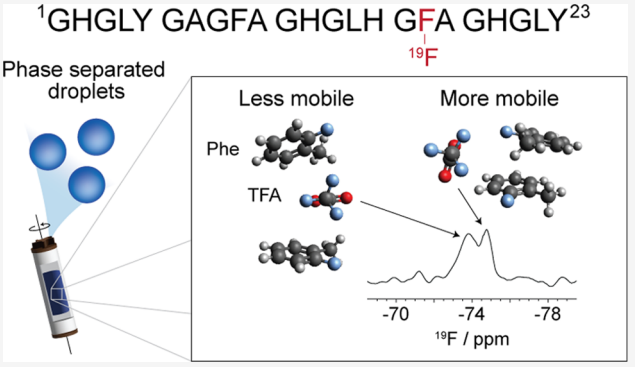

Liquid−liquid phase separation (LLPS) describes the demixing of a homogeneous biomolecule solution into two phases: a dilute, depleted phase and a dense, often concentration-rich phase[1,2] in the form of liquid droplets. Prevalent across broad research fields such as cell biology, material science, and soft matter,[3,4] LLPS is known to be driven by different system-specific factors such as temperature, pH, and ionic strength.[5,6] In particular, probing the effect of small molecules in the regulation of LLPS has gained growing interest, especially in the development of therapeutics where aberrant phase transitions serve as potential drug targets.[7−9] Small molecules may actively partition inside the droplets formed or induce changes to the local chemical environment,[10] including water-mediated structural changes,[11] indirectly modulating the phase boundaries. For example, 4,4′-dianilino-1,1′-binaphthyl-5,5′-disulfonic acid (bis-ANS) was found to promote heterotypic LLPS of TDP-43 LCD at concentrations significantly lower than its homotypic LLPS regime.[8] The cellular energy currency, adenosine triphosphate (ATP), recognized as a biological hydrotrope,[12] was found to additionally behave as a bivalent binder,[13] exerting opposing effects on the phase separation of FUS at different concentrations. Notably, the most popular small molecule regulator in the field,[7] 1,6-hexanediol, is commonly used as an additive to examine the dissolution of condensates driven by hydrophobic interactions. Salt ions, commonly found in buffer solutions, can not only regulate the nature of interactions within condensates[14] but may also, along with osmolytes[15] and metal ions,[16−19] induce structural changes.[20,21]

Trifluoroacetic acid (TFA) is a small molecule ubiquitously found in synthetic peptides and is the dominant ion-pairing reagent for efficient chromatographic separation by reverse-phase high-performance liquid chromatography (HPLC).[22,23] TFA is also used for the optimal removal of protecting groups and final cleavage from the resin for synthesized peptides.[24,25] Due to its high acidity, TFA can also efficiently solubilize certain proteins.[26,27] Here, we show that residual TFA (in its salt form, i.e., TFA^-, thereby also referred to as TFA) can significantly influence the phase separation characteristics of a chemically synthesized bioinspired peptide 1GHGLY GAGFA GHGLH GFA GHGLY23 (GY23) capable of undergoing LLPS primarily regulated by pH and ionic strength.[28] Strategically labeling the phenylalanine 17 (Phe-17) at the C2 ring position with ^{19}F isotope enabled us to employ background-free ^{19}F NMR spectroscopy to study structural and dynamic details of perturbations induced by TFA to glass-like mesoscale order (spanning several constituting peptide units) of GY23 in the dense phase.

The choice of Phe-17 for ^{19}F labeling was based on our previous observations that mutations at this position can

Received: July 4, 2024
Revised: October 17, 2024
Accepted: November 4, 2024

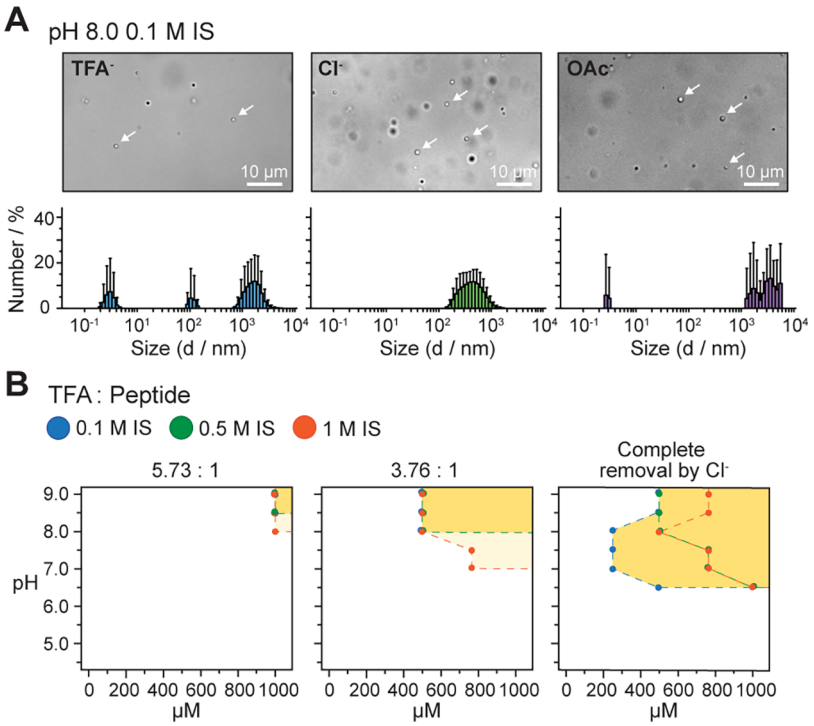

Figure 1. (A) Brightfield optical microscopy observation and DLS number-based size distributions of the phase separation behavior of unlabeled (i.e., no ^{19}F) GY23 with different counterions. Corresponding intensity- and volume-based plots can be found in Figure S2. (B) LLPS phase diagrams as a function of pH and GY23 concentration at varying TFA:peptide stoichiometry and ionic strength (colored dots). Unlabeled GY23 is used here. The LLPS conditions were determined by the appearance of droplets in brightfield microscopic images and in diagrams, demarcated by the dotted lines and colored space. IS: the ionic strength of the buffers tested. The maximum peptide concentration tested is 1 mM.

completely abolish dense gel formation and induce a significant time lag in the LLPS droplet buildup,[29] implying a significant role of this amino acid, especially in the condensed dense phase. The molecular mechanisms are currently completely unknown and potentially can be probed by external molecules capable of modulating the LLPS behavior of the peptide. Indeed, TFA shows markedly different LLPS modulating effects compared to related counterions (chloride, Cl^- and acetate, OAc^-) during the initial sample preparation of the condensed dense phase. Importantly, TFA is not typically considered a Hofmeister reagent with clear lyotropic and kosmotropic properties[30−32] and may even have opposing effects.[33] Previous studies showed its ability to refold proteins under strongly denaturing conditions, even at a comparatively low concentration.[34,35] Moreover, NMR-based structural studies showed specific, structural context-dependent interaction of TFA with a Phe residue in a refolded protein, modulating global protein structure.[34] Thus, we posited that TFA might modulate LLPS through specific interactions with aromatic moieties. Indeed, our experimental data reveal evidence for the proximity of TFA to Phe-17 in the condensed dense phase state of GY23 and its preferential localization to the aromatic rings. Our analysis indicates the simultaneous presence of two types of TFA and peptide complexes in the dense phase: the anisotropic, dipolar-ordered complexes and the mobile, chemically exchanging complexes. By utilizing the observed ^{19}F chemical shift disparities between TFA within the dipolar-ordered and chemically exchanging complexes, we employed quantum chemistry (QC) calculations to model the molecular configurations of the respective complexes. Our modeling shows that the tight complex may form when one TFA molecule intercalates between two stacked aromatic rings of Phe in the dense phase. This intercalation may modulate the interaction network required for condensed dense phase formation. At the same time, this intercalation may also impact the balance of interactions in the droplet phase, altering the size distribution of the dense droplets as well as the partitioning of the peptide between the dense phase and the bulk solvent. Thus, we propose that TFA can be used as a molecular probe, together with ^{19}F NMR, to reveal dynamic processes as well as ordered structures within the condensed dense phase, otherwise obscured in other techniques. This may be especially useful in liquid−liquid phase-separating peptide systems enriched in aromatic residues, which play central roles in LLPS of both native proteins and synthetic peptides.[4,28,36]

EXPERIMENTAL SECTION

Preparation of Peptides with Different TFA:Peptide Ratios. Peptides studied were synthesized and purified using standard methods, with details provided in the Supporting Information. To avoid batch variation, different aliquots were taken from the same purified batch of unlabeled peptide, dissolved in filtered Milli-Q to a concentration of 1 mg/mL, and treated with varying concentrations of hydrochloric acid (HCl). All aliquots were freeze-dried for one cycle before being solubilized in pH 3.5 10 mM acetic acid and subjected to solution state 1D ^{19}F NMR using an AVANCE Neo 400 MHz spectrometer (Bruker, Germany). External references of sodium trimethylsilylpropanesulfonate (DSS) and (pure) TFA were prepared with known concentrations. The integrals of TFA and peptide were subsequently determined for each aliquot using TopSpin 4.0.9 and compared with the references before computing the respective concentrations and TFA:peptide ratios, as derived in Figure 1A.

https://doi.org/10.1021/acs.analchem.4c03444
Anal. Chem. XXXX, XXX, XXX−XXX

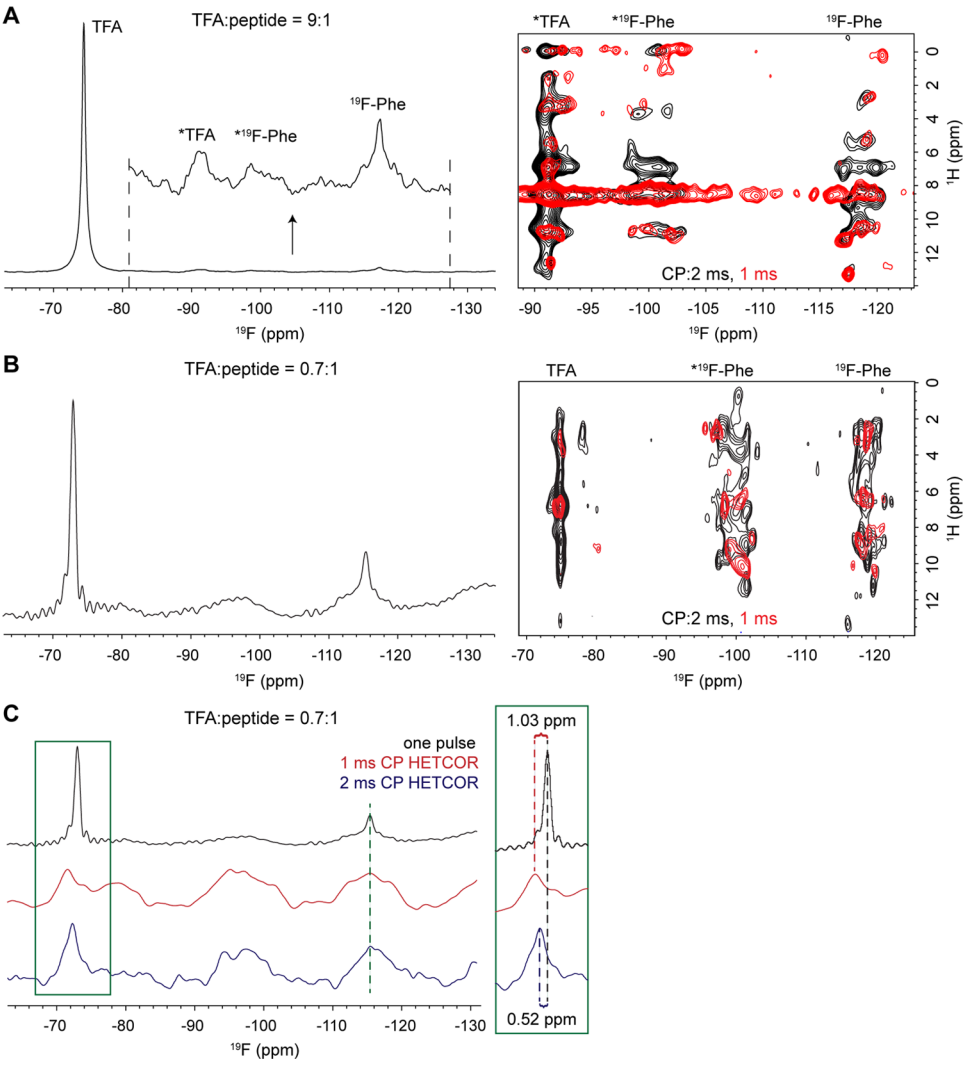

Figure 2. 1D ^{19}F MAS NMR spectrum and 2D overlay of $^{1}H-^{19}F$ cross-polarization (CP) HETCOR spectra using CP mixing times of 1 ms (red) and 2 ms (black) for samples with TFA:peptide ratio of (A) 9:1 and (B) 0.7:1. The pulse sequence used in the experiments is reported in Figure S3. (C) Overlay of one pulse 1D ^{19}F MAS spectra with two horizontal slices from corresponding 2D $^{1}H-^{19}F$ CP HETCOR of the sample with a TFA:peptide ratio of 0.7:1. Slices were taken at 7.01 ppm (^{1}H) corresponding to the resonances of the aromatic protons of Phe. Spinning sidebands are marked with an asterisk.

Exchange of TFA Counterion for Cl^- and OAc^-. For the complete removal of TFA, HCl was added, as described above, to a final concentration of 9 mM. Earlier optimization of this concentration was done to ensure no peptide degradation. Multiple cycles of freeze-drying, solubilization in filtered Milli-Q, and addition of HCl were subsequently performed. Next, to exchange Cl^- to OAc^-, reverse-phase HPLC was performed with the additive as 1% acetic acid. Desired fractions were identified, combined, and freeze-dried to remove any solvent.

Solid-State NMR Measurements. Details on sample preparation and rotor packing can be found in the Supporting Information. NMR measurements were performed by using a 600 MHz Bruker widebore spectrometer and a 1.9 mm solid probe capable of pulsing ^{1}H and ^{19}F at the same time. NMR chemical shifts were calibrated using adamantane, $C_{10}H_{16}$ (^{13}C, 37.85 and 28.46 ppm). No radiofrequency pulses were used for decoupling as MAS speed was sufficient. Samples were spun at 10 kHz (unless otherwise indicated) to maximize PDSD efficiency and introduce as little impact to the peptide gel structure from centrifugal force from rotor spinning as possible. The acquisition times for ^{19}F and ^{1}H were 6 and 1.6 ms, respectively. The probe temperature was set to 289 K for all measurements. CP measurements (Figure 2) were performed with 1 and 2 ms contact time and +1 Hartmann–Hahn condition. For 2D $^{19}F-^{19}F$ correlation spectra (Figure 3A,B), a 500 ms mixing time was used for $^{19}F-^{19}F$ dipolar recoupling. DARR measurements (Figure 3C,D) were performed at 30 kHz MAS and a 100 ms mixing time. HetNOE measurements (Figure 4) were performed at a 200 ms NOE time and a MAS of 30 kHz.

Quantum Chemistry Calculations and Computation of Predicted Chemical Shift Perturbations. Quantum chemistry calculations were performed using Gaussian 16.[37] Starting configurations were first prepared using the molecule editor Avogadro 1.2.0.[38] Geometric optimizations were performed using the basis set wB97XD/cc-pVDZ, chosen for its reasonable computational costs. As calculations were performed using the TFA anion, diffuse functions were included in the job route. In addition, from preliminary calculations (data not shown) and experimental data, the

https://doi.org/10.1021/acs.analchem.4c03444
Anal. Chem. XXXX, XXX, XXX−XXX

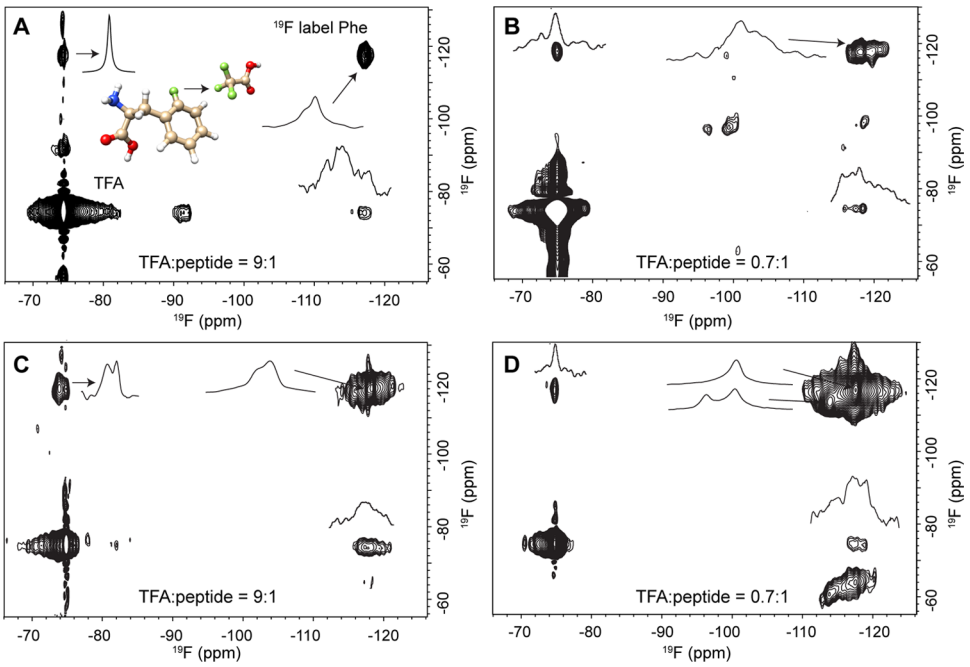

Figure 3. 2D ^{19}F−^{19}F correlation spectra of the condensed dense phase samples with a (A) TFA:peptide ratio of 9:1 and a (B) TFA:peptide ratio of 0.7:1. Dipolar-assisted rotational resonance (DARR) spectra for a (C) TFA:peptide ratio of 9:1 and a (D) TFA:peptide ratio of 0.7:1.

solvation of the system was determined to be essential. Hence, all calculations were performed in a water cavity with an additional keyword, SCRF, in the job route. All optimized structures were subsequently subjected to further NMR calculations using the gauge-independent atomic orbital (GIAO) method with the same basis set and conditions per geometric optimizations. No scaling was performed, as only difference values were considered. All output structures were again examined by using Avogadro 1.2.0.

RESULTS

Impact of TFA on the GY23 LLPS Behavior. Brightfield microscopy and dynamic light scattering (DLS) show that even traces of TFA can significantly impact the LLPS behavior of the GY23 peptide system reported in previous studies.[28,29] Figure 1 shows that the presence of TFA at TFA:peptide stoichiometry exceeding 1:1 can significantly narrow the conditions in the phase transition diagrams, where LLPS was microscopically observable as compared to Cl^- as the counterion. DLS analyses showed that in the presence of TFA, in addition to the main fraction of droplets with a diameter of about 1−2 μm, two smaller-sized populations of droplets with diameters between 0.1 and 10 nm and around 100 nm were observed, respectively. The Cl^- counterion was subsequently exchanged by HPLC to OAc^- (CH_3COO^-), a closer chemical counterpart of TFA. Although some variation in droplet size distribution was observed, OAc^- counterion resulted in a more similar LLPS behavior of GY23 compared to TFA. These results indicate rather specific TFA interactions with the peptide that may impact the structure of the dense phase, which are likely absent when TFA is replaced by Cl^-. This effect can be attributed more to the unique presence of three fluorine atoms in TFA and less to its overall chemical structure.

The significant differences between TFA^- and Cl^- counterions led us to investigate their effects on phase separation more systematically. Varying ratios were obtained by the controlled addition of hydrochloric acid (HCl) to the unlabeled peptide with a single freeze-drying step to ensure that some TFA remained in the dense phase, and the ratios were then determined. As seen from Figure 1B, with increasing removal of TFA, the critical concentrations at which droplets were identified shifted toward lower values at the same pH, and the pH boundary also expanded toward pH 6.5. Interestingly, with the complete removal of TFA by Cl^-, its phase separation does not correlate linearly with the ionic strength, with droplets observed with lower peptide concentrations at lower ionic strengths instead. The lowest TFA:peptide ratio, which did not significantly impact the peptide's ability to form a condensed dense phase, was determined to be 0.7:1. Through standard purification methods, without intentionally removing TFA, a TFA:peptide ratio of around 9:1 was observed. We used these two TFA:peptide ratios for ^{19}F NMR-based studies of the perturbations of the dense phase formed by GY23.

^{1}H−^{19}F CP HETCOR. The dipole-ordered, rigid configuration of TFA in proximity to Phe was characterized by the acquisition of the ^{1}H−^{19}F HETCOR spectra for the TFA:peptide ratio of 9:1 and 0.7:1 (Figure 2). The polarization transfer between ^{1}H and ^{19}F was achieved by using the continuous wave (CW) cross-polarization (CP) technique, thus highlighting exclusively dipolar-ordered complexes. Figure 2A shows the 1D ^{19}F NMR spectrum of the 9:1 sample with excess TFA, showing the dominant TFA resonance at −75 ppm. In contrast, a significantly smaller resonance was observed in the downfield region of −120 ppm, corresponding to that of ^{19}F-Phe. The strong bulk TFA signal at −75 ppm overlaps with the peak originating from dipolar-ordered TFA at −74 ppm. This overlap is resolved in the 2D ^{1}H−^{19}F spectra, where we established the presence of the dipolar-ordered complex using TFA spinning sidebands at −90 ppm.

The analysis of the 2D HETCOR spectra overlaid at different mixing times in Figure 2A,B indicates that the spatial proximity of TFA to GY23 proton spins in the dipolar-ordered

https://doi.org/10.1021/acs.analchem.4c03444
Anal. Chem. XXXX, XXX, XXX−XXX

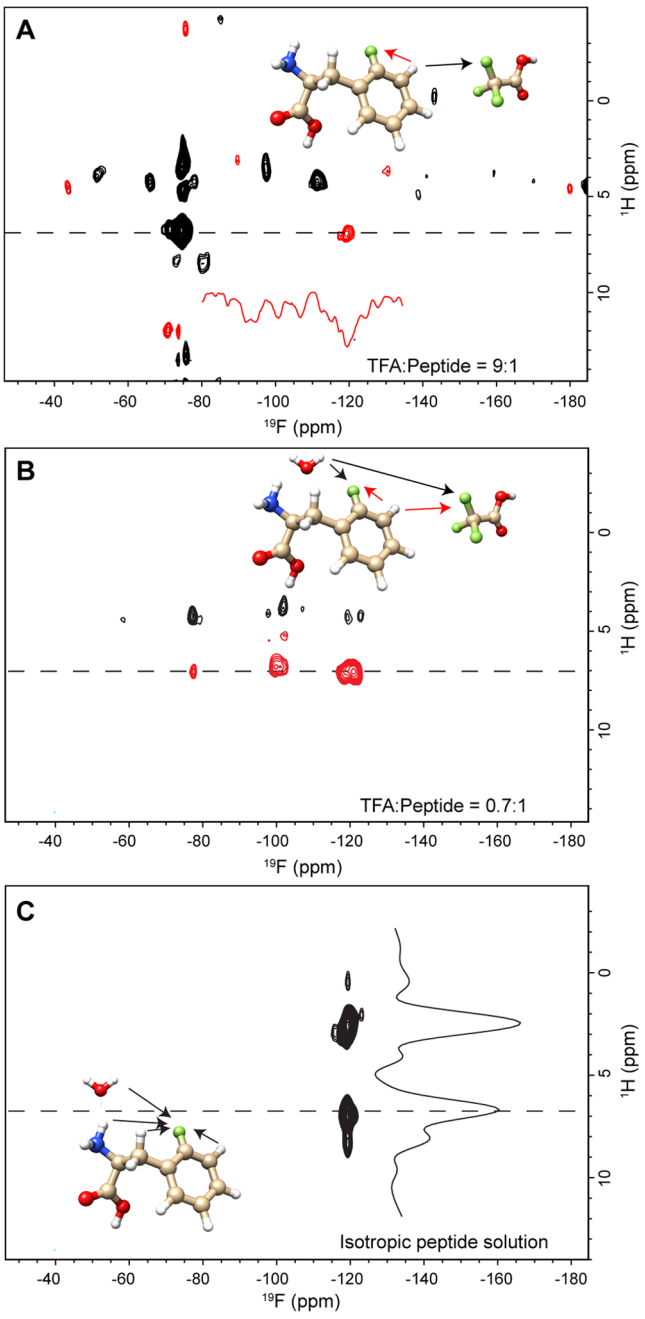

Figure 4. 2D ^{1}H−^{19}F HetNOE spectra recorded on samples with different TFA:peptide ratios. The pulse sequence is included in Figure S3. (A) ^{1}H-Phe/^{19}F-Phe cross-peak showed a different sign than ^{1}H-Phe/TFA peak for sample TFA:peptide = 9:1. (B) Mixing peaks showed the same negative phase in TFA:peptide = 0.7:1. (C) Spectrum was recorded by using the isotropic peptide solution at pH 3.5. The $w_1(^{1}H)$ profile taken at −120 ppm (^{19}F-Phe) exhibits three groups of cross-peaks at $\delta\{^{1}H\}$ = 2.41, 6.95, and 8.41 ppm.

complexes is modulated by their relative concentrations. The higher TFA concentration results in stronger cross-peaks between ^{19}F-TFA and amide protons (8.3−8.5 ppm). Lowering the TFA concentration results in the corresponding increase in the amplitude of the cross-peaks between ^{19}F-TFA and the aromatic protons (6−7 ppm). ^{1}H−^{19}F polarization transfer simulations performed by SIMPSON (see Figure S4) indicate that ^{19}F spins in the fully rigid system can be polarized by ^{1}H spins within a 5 Å radius and thus might indicate a dipolar semirigid meso-order or glass-like order spanning at least several amino acids of the peptide. This radius might be reduced due to the dynamic averaging of the ^{1}H−^{19}F and ^{1}H−^{1}H dipolar couplings caused by the intramolecular flexibility.

2D PDSD and DARR Spectroscopy. An interplay between the anisotropic dipolar-coupled and isotropic dynamic complexes of TFA with GY23 in the dense phase was studied by 2D homonuclear polarization transfer proton-driven spin diffusion (PDSD) and dipolar-assisted rotational resonance (DARR) experiments under MAS conditions. While both direct ^{19}F to ^{19}F dipolar coupling and spin−spin cross-relaxation between ^{19}F spins can contribute to the PDSD signals, these relative contributions can be modulated by employing DARR mixing sequences. Thus, a comparison of the PDSD and DARR spectra at different TFA:peptide ratios might help to differentiate ^{19}F chemical shift differences in dipolar-ordered and dynamic complexes. Figure 3 shows PDSD and DARR spectra measured at different TFA:peptide ratios. In all of the spectra, two dominant diagonal peaks, corresponding to ^{19}F-TFA and ^{19}F-Phe, are observed. At a higher TFA to peptide ratio, a narrow $w_2(^{19}F)$ profile of the cross-peak correlating the ^{19}F-TFA resonance to ^{19}F-Phe shows a single maximum at −75 ppm (Figure 3A). Lowering the TFA concentration resulted in a more broadened profile with an apparent maximum at −74 ppm (Figure 3B), indicating ^{19}F chemical shifts corresponding to the dynamic and ordered complexes, respectively. With no radiofrequency irradiation involved in the PDSD mixing scheme, the transfer of magnetization is dominated by the dynamic exchange of the mobile components. In contrast, DARR recoupling provides more emphasis on polarization transfer due to direct ^{19}F−^{19}F dipolar coupling. The ^{19}F-TFA cross-peak profile (Figure 3C) measured using DARR at the high TFA content shows two constituting resonance lines with maxima at −75 and −74 ppm. DARR spectrum measured at the lower TFA content (Figure 3D) showed a relatively homogeneous profile of ^{19}F-TFA cross-peak, with the maximum at −74 ppm corresponding to the dipolar-ordered complex. Therefore, we hypothesize that the ^{19}F-TFA resonance at −75 ppm visible in the PDSD spectra arises from the exchanging bulk (free) TFA with TFA located near the peptide. The ^{19}F-TFA resonance at −75 ppm, which can be observed at the lower TFA concentration and under recoupling conditions in DARR, suggests that TFA is also "trapped" in a more solid-like state, characterized by significant dipolar order.

Heteronuclear NOEs. The dynamic complex of TFA and GY23 was further studied by 2D ^{1}H−^{19}F HetNOE spectroscopy, where the observed cross-peaks can be exclusively attributed to the spin−spin cross-relaxation and chemical exchange processes between ^{19}F spins of TFA and Phe and other moieties in the peptide lattice or the bulk solvent. In the dense phase and at high TFA concentration, the cross-peaks of ^{19}F-TFA at −74 ppm and ^{19}F-Phe peak at −120 ppm to the aromatic protons at 6.92 ppm exhibit opposite signs (Figure 4A), suggesting differences in the effective rotational correlation time associated with the dynamics of the respective moieties. However, at the lower TFA:peptide ratio, the NOESY cross-peaks between ^{19}F-TFA and aromatic protons are of the same sign as those of ^{19}F-Phe to the Phe-17 protons (Figure 4B). This suggests that the excess of TFA in the dense phase is in fast (in NMR time scale) exchange with the bulk solvent while still mobile but exhibits slower exchange with

https://doi.org/10.1021/acs.analchem.4c03444
Anal. Chem. XXXX, XXX, XXX−XXX

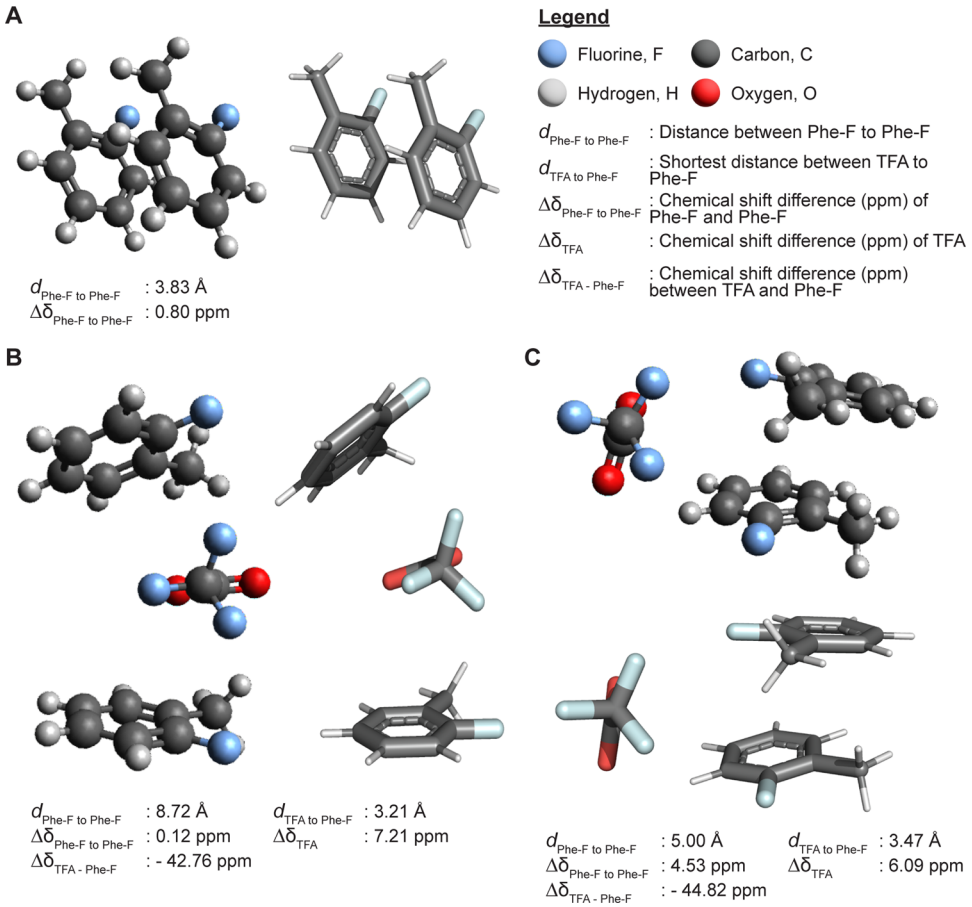

Figure 5. Energy-optimized geometries and ^{19}F chemical shift variations of (A) with two stacked toluene (methylbenzene) molecules substituted with a fluorine atom at the methylbenzene ring used to model the phenylalanine residue. (B) Intercalated and (C) lateral configuration of TFA with two fluorinated toluene molecules calculated using Gaussian 16.[37] The ^{19}F chemical shift variations, $\Delta\delta$ (ppm), are reported as the difference of the calculated ^{19}F chemical shifts in the reported configuration and with the constituent molecules displaced from each other by more than 11 Å and averaged for the three fluorine atoms of TFA. Additional explored geometries are in Figure S6.

Phe-17, thus forming complexes with the stoichiometric (equimolar) amount of interactants. At pH 3.5, when no LLPS was observed, ^{19}F-Phe-17 shows NOESY cross-peaks attributed to the protons of the aromatic ring of Phe-17 as well as its backbone and methylene protons, a pattern expected in the unstructured monomeric and isotropically tumbling peptide in solution. The spin dynamics simulations of the 2D ^{1}H−^{19}F HetNOE spectra using QSim[39] (see SI and Figure S5) showed that HetNOE sign reversal occurs at the effective rotational correlation time of about 300 ps. Thus, the dynamic time scales of the TFA/Phe-17 complexes can fall in the 100−300 ps range with an excess of TFA (the lower boundary corresponds to the free TFA in water) and above 300 ps for the stoichiometric (equimolar) complexes. The simulations show that the NOE cross-peaks in homonuclear 2D ^{19}F−^{19}F PDSD spectra under MAS conditions show no sign reversal as a function of the rotational correlation time as it is observed experimentally (Figure 3).

QC Modeling of Dipolar-Ordered TFA/Phe Complexes. The variation in ^{19}F chemical shifts observed in dipolar-ordered and isotropic complexes is utilized as a guide to elucidate potential geometries of TFA and Phe complexes. To reduce the molecular configurational space, the ^{19}F-substituted Phe residue was modeled with fluorinated toluene (methylbenzene) (Figure 5A). Since the aromatic ring clustering configuration of Phe residues was assumed to contribute significantly to the stabilization of the condensed dense phase,[29] and specifically, $\pi-\pi$ interactions arising from aromatic rings recognized as a major contributor to phase separation,[40] we explored three-partite configurations including one TFA and two stacked toluene molecules. The calculated variation of the ^{19}F chemical shift of TFA in the intercalated geometry (Figure 5B) as opposed to the lateral geometry (Figure 5C) was +1.12 ppm (7.21−6.09 ppm), well matching the experimental observation of the ^{19}F chemical shift variation of TFA between the dipolar-ordered (−74 ppm) and mobile (−75 ppm) complexes.

Our modeling indicates that the intercalated configuration of TFA might provide a sufficiently rigid scaffold to maintain the mesoscale (spanning several peptides) order, resulting in the persistence of intermolecular nonaveraged anisotropic dipolar couplings in the NMR time scale. On the other hand, the lateral configuration of TFA relative to the stacked or individual aromatic rings might provide a transiently stable and mobile complex in fast exchange with the solvent. In general, the presence of the TFA molecule and its orientation can influence the configuration of the interacting aromatic moieties relative to one another, which might modulate the LLPS processes.

https://doi.org/10.1021/acs.analchem.4c03444
Anal. Chem. XXXX, XXX, XXX−XXX

DISCUSSION

The ^{19}F NMR spectroscopic observations of the TFA/GY23 peptide system under LLPS conditions revealed the presence of several dynamically distinct TFA to Phe-17 complexes. The dipolar-ordered, anisotropic rigid complex was observed in the cross-polarization transfer-based ^{1}H−^{19}F HETCOR spectroscopy in which one TFA molecule intercalates between two aromatic rings of Phe residues, potentially stemming from different peptide units forming the dense phase lattice. The formation of such mesoscale-ordered complexes probably constitutes the main dense phase modulation mechanism of TFA. In the absence of TFA, the $\pi-\pi$ stacking of the aromatic residues, which also includes Tyr to Tyr stacking, may define the network of interactions stabilizing the molecular order in the dense phase spanning at least several peptides. This rigid complex coexists in the dense phase with more dynamic, isotropically tumbling complexes manifesting themselves via spin−spin cross-relaxation processes. At the higher than equimolar stoichiometry of TFA:peptide ratio, the effective rotational correlation time of TFA/Phe complex is in the range of 100−300 ps, which is slower than that of TFA in the bulk solvent, indicating affinity of TFA to Phe in the peptide. The removal of the excess TFA reveals the presence of yet slower-tumbling isotropic TFA/Phe complex with an effective rotational correlation time longer than 300 ps. In this slower-tumbling isotropic complex, Phe and TFA exhibit similar dynamics and potentially are in a well-defined configuration. Guided by the ^{19}F chemical shift variation, QC modeling predicts that in the tight complex, TFA intercalates between two interacting aromatic rings, and more dynamic complexes might form when TFA is more laterally positioned to the stacked aromatic rings.

The underlying reason why TFA and OAc lead to the stabilization of the condensed dense phase is still debatable. Beyond the Hofmeister effect, as mentioned earlier, the counterions present may also participate in other interactions that may not follow standard Hofmeister ordering. Here, we would like to recapitulate a significant observation during sample preparation where, in stark contrast to Cl^-, a stable condensed dense phase could only be achieved by TFA and its similar chemical counterpart, OAc^-, albeit with slightly more salt needed in the buffer for the latter. Moreover, the differing presence of intermediate populations of phase-separated GY23, as shown in Figure 1, is reminiscent of the formation of helical intermediates only when TFA was present as a counterion for amyloid-β peptides.[41] Coupled with our experimental findings, we therefore believe van der Waals forces may be at play. The calculated values (through quantum chemistry[37,42] and parsed by Multiwfn[43]) of isotropic average polarizability (Table S1) of TFA and OAc^- were similar but significantly higher than Cl^-. Higher polarizabilities generally lead to stronger van der Waals forces due to greater ease of distorting the electron cloud and inducing dipolar moment.[44,45] Notably, van der Waals forces are significantly associated with interactions between aromatic rings.[46,47] One of the driving forces in several phase-separating systems is the specific presence of such clusters[48,49] that also play crucial roles in protein stabilization,[50] protein interactions,[47,51] and fibril formation.[52] However, we would also like to emphasize the collective and statistical nature of contributions stemming from these aromatic clusters over pairwise or individual interactions, as demonstrated in several phase-separated systems.[49,53,54] Therefore, we envision the impact of TFA on phase separation for different systems to vary due to the strength of their underlying interactions, where stronger driving forces may diminish its overall impact.

TFA has often been regarded simply as a contaminant resulting from purification processes, and much research focus has been on its removal and detrimental effects. However, in this study, similar to how fluorinated alcohol, trifluoroethanol (TFE) was used as a probe molecule to monitor the kinetics and spatial evolution of the dense phase formation in LLPS,[55] we used TFA within the peptide system to gain unique insights on the structure and dynamics within the condensed dense phase. The condensed dense phase primarily consists of dipolar-ordered complexes, contributing to its mesoscale order and imparting rigidity. Importantly, the observation of slow and fast exchanging dynamic complexes between TFA and Phe provides compelling evidence for not only the existence of diffusive regions within the condensed dense phase but also its immediate adjacent localization to the dipolar-ordered structural scaffold. This hints at a possibly micro/nanoporous structure within droplets where the internal surfaces facilitate the exchange of dynamic complexes of TFA with the bulk solvent, further underscoring our NMR observations. Therefore, as we have demonstrated in our study, when the chemical grammar of small molecules can be elucidated,[56] small molecules such as TFA can also serve as valuable molecular probes in advancing our comprehension of the LLPS-related dense phase, expanding the range of condensates which can be structurally studied at atomic resolution.

CONCLUSIONS

Probing specific interactions within the dense phase is challenging. Such interactions are not only transient and dynamic but span large time scales, not easily observable in a single technique. Furthermore, the high viscosity of the condensates renders them inaccessible to solution NMR methods, while conventional ^{13}C-based solid-state NMR techniques are ineffective due to the reduced dipolar order within. For the first time, to the best of our knowledge, by adding a single Phe ^{19}F-labeled site within the aromatic ring and employing TFA as a molecular probe, we were able to use background-free ^{19}F solid-state NMR methods to uncover the presence of both dipolar-ordered and dynamically fluctuating complexes within the dense phase. The presence of dipolar-ordered complexes most likely contributes to the mesoscale order of the dense phase and imparts rigidity. More significantly, the porous nature within droplets, as hinted at by our data, represents a fundamental deviation from the perceived uniform internal densities of biocondensates. This raises fundamental questions about the functional implications for macroscale properties, which require further investigation.

ASSOCIATED CONTENT

Supporting Information

The Supporting Information is available free of charge at https://pubs.acs.org/doi/10.1021/acs.analchem.4c03444.

Additional details on materials and methods, ^{19}F solution state 1D NMR spectra of labeled peptides with varying TFA concentrations, data from dynamic light scattering of peptide after induction of phase separation with different counterions, pulse sequences used for CP HETCOR and HetNOESY experiments, SIMPSON simulations of ^{1}H−^{19}F cross-polarization

https://doi.org/10.1021/acs.analchem.4c03444
Anal. Chem. XXXX, XXX, XXX−XXX

efficiency, QSim simulations of F−F and H−F NOESY, additional interacting configurations of TFA molecule(s) with Phe side chain(s) from quantum chemistry, and different geometries of Phe side chain(s) with predicted NMR chemical shifts from quantum chemistry and computed values of isotropic average polarizability for the counterions discussed in this study (PDF)

AUTHOR INFORMATION

Corresponding Authors

Ali Miserez − *School of Biological Sciences, Nanyang Technological University, 637551, Singapore; Centre for Sustainable Materials (SusMat), School of Materials Science and Engineering, Nanyang Technological University (NTU), 637553, Singapore;* orcid.org/0000-0003-0864-8170; Email: ali.miserez@ntu.edu.sg

Kai Xue − *Centre of High Field NMR Spectroscopy and Imaging and School of Physical and Mathematical Sciences, Nanyang Technological University, 637371, Singapore;* Email: kai.xue@ntu.edu.sg

Konstantin Pervushin − *School of Biological Sciences, Nanyang Technological University, 637551, Singapore;* Email: kpervushin@ntu.edu.sg

Authors

Jessica Lim − *School of Biological Sciences, Nanyang Technological University, 637551, Singapore;* orcid.org/0009-0005-6822-921X

SzeYuet Chin − *School of Biological Sciences, Nanyang Technological University, 637551, Singapore; Centre of High Field NMR Spectroscopy and Imaging, Nanyang Technological University, 637371, Singapore*

Complete contact information is available at: https://pubs.acs.org/10.1021/acs.analchem.4c03444

Author Contributions

K.P., K.X., and A.M. conceived the study, designed the methodologies, provided the reagents and instrumentation, reviewed, and edited the manuscript. K.X., S.Y.C., and J.L. conducted the experiments and collected the data. All authors analyzed the data. K.P., K.X., J.L., and S.Y.C. wrote the original draft. K.X. and J.L. prepared the figures. K.P. coordinated the project. A.M. and K.P. secured the funding. All authors have given approval to the final version of the manuscript.

Notes

The authors declare no competing financial interest.

ACKNOWLEDGMENTS

We would like to thank Nanyang Technological University for the funding of NMR measurements at the NTU Centre of High-Field NMR Spectroscopy and Imaging. This work was funded by the Singapore Ministry of Education (MOE) through an Academic Research Fund (AcRF) Tier 3 grant (grant # MOE 2019-T3-1-012). We would also like to thank Dr. Yuguang Mu from the School of Biological Sciences, Nanyang Technological University, for providing access to his computational resources for all quantum chemistry calculations in this work.

REFERENCES

(1) Alberti, S. *Curr. Biol.* **2017**, *27* (20), R1097−R1102.
(2) Shin, Y. *Mol. Cells* **2022**, *45* (1), 6−15.
(3) Shil, S.; Tsuruta, M.; Kawauchi, K.; Miyoshi, D. *BioTech* **2023**, *12* (2), 26.
(4) Harrington, M. J.; Mezzenga, R.; Miserez, A. *Nat. Rev. Bioeng.* **2024**, *2* (3), 260−278.
(5) Maruri-Lopez, I.; Chodasiewicz, M. *Curr. Opin. Plant. Biol.* **2023**, *74*, No. 102385.
(6) Vendruscolo, M.; Fuxreiter, M. Towards sequence-based principles for protein phase separation predictions. *Curr. Opin. Chem. Biol.* **2023**, *75*102317.
(7) Li, S.; Wang, Y.; Lai, L. *Acta Biochim. Biophys. Sin.* **2023**, *55* (7), 1075−1083.
(8) Babinchak, W. M.; Dumm, B. K.; Venus, S.; Boyko, S.; Putnam, A. A.; Jankowsky, E.; Surewicz, W. K. *Nat. Commun.* **2020**, *11* (1), No. 5574.
(9) Klein, I. A.; Boija, A.; Afeyan, L. K.; Hawken, S. W.; Fan, M.; Dall'Agnese, A.; Oksuz, O.; Henninger, J. E.; Shrinivas, K.; Sabari, B. R.; et al. *Science* **2020**, *368* (6497), 1386−1392.
(10) Hilaire, M. R.; Abaskharon, R. M.; Gai, F. *J. Phys. Chem. Lett.* **2015**, *6* (13), 2546−2553.
(11) Ribeiro, S. S.; Samanta, N.; Ebbinghaus, S.; Marcos, J. C. *Nat. Rev. Chem.* **2019**, *3* (9), 552−561.
(12) Patel, A.; Malinovska, L.; Saha, S.; Wang, J.; Alberti, S.; Krishnan, Y.; Hyman, A. A. *Science* **2017**, *356* (6339), 753−756.
(13) Kang, J.; Lim, L.; Song, J. *Biochem. Biophys. Res. Commun.* **2018**, *504* (2), 545−551.
(14) Krainer, G.; Welsh, T. J.; Joseph, J. A.; Espinosa, J. R.; Wittmann, S.; de Csillery, E.; Sridhar, A.; Toprakcioglu, Z.; Gudiskyte, G.; Czekalska, M. A.; et al. *Nat. Commun.* **2021**, *12* (1), No. 1085, DOI: 10.1038/s41467-021-21181-9.
(15) Celinski, S. A.; Scholtz, J. M. *Protein Sci.* **2002**, *11* (8), 2048−2051.
(16) Hong, K.; Song, D.; Jung, Y. *Nat. Commun.* **2020**, *11* (1), No. 5554.
(17) Xu, B.; Huang, S.; Liu, Y.; Wan, C.; Gu, Y.; Wang, D.; Yu, H. *J. Biol. Chem.* **2022**, *298*, No. 101469.
(18) Sołtys, K.; Tarczewska, A.; Bystranowska, D. *Biochim. Biophys. Acta, Mol. Cell Res.* **2023**, *1870* (8), No. 119567.
(19) Das, B.; Roychowdhury, S.; Mohanty, P.; Rizuan, A.; Chakraborty, J.; Mittal, J.; Chattopadhyay, K. *EMBO J.* **2023**, *42* (2), No. e111185.
(20) Korolev, N. *BioEssays* **2021**, *43* (1), No. e2000108.
(21) Younan, N. D.; Klewpatinond, M.; Davies, P.; Ruban, A. V.; Brown, D. R.; Viles, J. H. *J. Mol. Biol.* **2011**, *410* (3), 369−382.
(22) Pearson, J. D.; McCroskey, M. C. *J. Chromatogr. A* **1996**, *746*, 277−281.
(23) Cai, B.; Li, J. *Anal. Chim. Acta* **1999**, *399*, 249−258.
(24) Roux, S.; Zekri, E.; Rousseau, B.; Paternostre, M.; Cintrat, J. C.; Fay, N. *J. Pept. Sci.* **2008**, *14* (3), 354−359.
(25) Kiso, Y.; Yajima, H. 2 - Amide Formation, Deprotection, and Disulfide Formation in Peptide Synthesis. In *Peptides*; Gutte, B., Ed.; Academic Press, 1995; pp 39−91.
(26) Katz, J. J. *Nat. Chem. Biol.* **1954**, *174* (4428), No. 509.
(27) Burra, G.; Thakur, A. K. *Anal. Biochem.* **2016**, *494*, 23−30.
(28) Gabryelczyk, B.; Cai, H.; Shi, X.; Sun, Y.; Swinkels, P. J. M.; Salentinig, S.; Pervushin, K.; Miserez, A. *Nat. Commun.* **2019**, *10* (1), No. 5465.
(29) Lim, J.; Kumar, A.; Low, K.; Verma, C. S.; Mu, Y.; Miserez, A.; Pervushin, K. *J. Phys. Chem. B* **2021**, *125* (25), 6776−6790.
(30) Baldwin, R. L. *Biophys. J.* **1996**, *71* (4), 2056−2063.
(31) Collins, K. D.; Washabaugh, M. W. *Q. Rev. Biophys.* **1985**, *18* (4), 323−422.
(32) Zhang, Y.; Cremer, P. S. *Curr. Opin. Chem. Biol.* **2006**, *10* (6), 658−663.
(33) Sikora, K.; Jaskiewicz, M.; Neubauer, D.; Migon, D.; Kamysz, W. The role of counter-ions in peptides-An overview. *Pharmaceuticals* **2020**, *13* (12). DOI: 442.
(34) Pervushin, K.; Wider, G.; Iwai, H.; Wüthrich, K. *Biochemistry* **2004**, *43* (44), 13937−13943.

(35) Goto, Y.; Takahashi, N.; Fink, A. L. *Biochemistry* **1990**, *29* (14), 3480−3488.
(36) Abbas, M.; Lipiński, W. P.; Nakashima, K. K.; Huck, W. T. S.; Spruijt, E. *Nat. Chem.* **2021**, *13* (11), 1046−1054.
(37) *Gaussian 16*; Gaussian, Inc: Wallingford, CT, 2016. https://gaussian.com/gaussian16/ (accessed June 12, 2023).
(38) Hanwell, M. D.; Curtis, D. E.; Lonie, D. C.; Vandermeersch, T.; Zurek, E.; Hutchison, G. R. *J. Cheminf.* **2012**, *4* (1), No. 17, DOI: 10.1186/1758-2946-4-17.
(39) Helgstrand, M.; Allard, P. Q. *J. Biomol. NMR.* **2004**, *30*, 71−80.
(40) Vernon, R. M.; Chong, P. A.; Tsang, B.; Kim, T. H.; Bah, A.; Farber, P.; Lin, H.; Forman-Kay, J. D. *elife* **2018**, *7*, No. e31486, DOI: 10.7554/eLife.31486.
(41) Benseny-Cases, N.; Klementieva, O.; Cladera, J. *In vitro* Oligomerization and fibrillogenesis of amyloid-beta peptides. In *Protein Aggregation and Fibrillogenesis in Cerebral and Systemic Amyloid Disease*; Harris, J. R., Ed.; Springer: Netherlands, 2012; pp 53−74.
(42) Hickey, A. L.; Rowley, C. N. *J. Phys. Chem. A* **2014**, *118* (20), 3678−3687.
(43) Lu, T.; Chen, F. *J. Comput. Chem.* **2012**, *33* (5), 580−592.
(44) Rossi, M.; Tkatchenko, A.; Rempe, S. B.; Varma, S. *Proc. Natl. Acad. Sci. U.S.A.* **2013**, *110* (32), 12978−12983.
(45) Tao, J.; Rappe, A. M. *J. Chem. Phys.* **2016**, *144* (3), No. 031102.
(46) Hunter, C. A. *Chem. Soc. Rev.* **1994**, *23* (2), 101−109.
(47) Anjana, R.; Vaishnavi, M. K.; Sherlin, D.; Kumar, S. P.; Naveen, K.; Kanth, P. S.; Sekar, K. *Bioinformation* **2012**, *8*, 1220−1224.
(48) Holehouse, A. S.; Ginell, G. M.; Griffith, D.; Boke, E. *Biochemistry* **2021**, *60* (47), 3566−3581.
(49) Martin, E. W.; Holehouse, A. S.; Peran, I.; Farag, M.; Incicco, J. J.; Bremer, A.; Grace, C. R.; Soranno, A.; Pappu, R. V.; Mittag, T. *Science* **2020**, *367*, 694−699.
(50) Makwana, K. M.; Mahalakshmi, R. *Protein Sci.* **2015**, *24* (12), 1920−1933.
(51) Lanzarotti, E.; Defelipe, L. A.; Marti, M. A.; Turjanski, A. G. *J. Cheminform.* **2020**, *12* (1), No. 30.
(52) Pachahara, S. K.; Nagaraj, R. *Biochem. Biophys. Rep.* **2015**, *2*, 1−13.
(53) Lin, Y.; Currie, S. L.; Rosen, M. K. *J. Biol. Chem.* **2017**, *292* (46), 19110−19120.
(54) Kato, M.; Han, T. W.; Xie, S.; Shi, K.; Du, X.; Wu, L. C.; Mirzaei, H.; Goldsmith, E. J.; Longgood, J.; Pei, J.; et al. *Cell* **2012**, *149* (4), 753−767.
(55) Bramham, J. E.; Golovanov, A. P. *Nat. Commun.* **2022**, *13* (1), No. 1767.
(56) Kilgore, H. R.; Young, R. A. *Nat. Chem. Biol.* **2022**, *18*, 1298.

https://doi.org/10.1021/acs.analchem.4c03444
Anal. Chem. XXXX, XXX, XXX−XXX